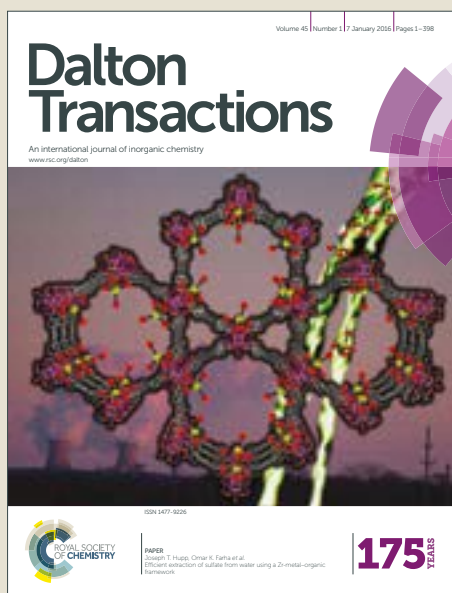


Dalton Transactions

Accepted Manuscript



This article can be cited before page numbers have been issued, to do this please use: M. Jamshidi, M. Babaghasabha, H. R. Shahsavari and S. M. Nabavizadeh, *Dalton Trans.*, 2017, DOI: 10.1039/C7DT03599C.



This is an Accepted Manuscript, which has been through the Royal Society of Chemistry peer review process and has been accepted for publication.

Accepted Manuscripts are published online shortly after acceptance, before technical editing, formatting and proof reading. Using this free service, authors can make their results available to the community, in citable form, before we publish the edited article. We will replace this Accepted Manuscript with the edited and formatted Advance Article as soon as it is available.

You can find more information about Accepted Manuscripts in the [author guidelines](#).

Please note that technical editing may introduce minor changes to the text and/or graphics, which may alter content. The journal's standard [Terms & Conditions](#) and the ethical guidelines, outlined in our [author and reviewer resource centre](#), still apply. In no event shall the Royal Society of Chemistry be held responsible for any errors or omissions in this Accepted Manuscript or any consequences arising from the use of any information it contains.

Influence of Thiolate Ligands on Luminescent Properties of Cycloplatinated(II) Complexes

Mahboubeh Jamshidi,^a Mojgan Babaghasabha,^b Hamid R. Shamsavari^{b*} and S. Masoud Nabavizadeh^{a*}

^aDepartment of Chemistry, College of Sciences, Shiraz University, Shiraz 71454, Iran.

^bDepartment of Chemistry, Institute for Advanced Studies in Basic Sciences (IASBS), Yousef Sobouti Blvd., Zanjan 45137-66731, Iran.

*Email: shamsavari@iasbs.ac.ir. (H.R.S.); nabavizadeh@shirazu.ac.ir. (S.M.N).

Abstract:

Complexes [Pt(C[^]N)(PPh₃)Cl] (C[^]N = bzq (7,8-benzoquinoliny, **A**) and ppy (2-phenylpyridinyl, **B**)) were reacted with various thiolate ligands to afford complexes [Pt(C[^]N)(PPh₃)(κ⁻¹-S-SR)], C[^]N = bzq, R = SPh (thiophenolate, **1a**); C[^]N = ppy, R = SPh (**1b**); C[^]N = bzq, R = Spy (pyridine-2-thiolate, **2a**); C[^]N = ppy, R = Spy (**2b**); C[^]N = bzq, R = SpyN (pyrimidine-2-thiolate, **3a**); C[^]N = ppy, R = SpyN (**3b**). The complexes **1-3** were characterized by NMR spectroscopy, and the solid-state structures of **1a** and **2a** which determined by X-ray diffraction methods. Replacing chloride ligand with electron-rich thiolates change the lowest-energy singlet and triplet excited states to ones that feature charge transfer from the thiolate (mixed with some metal character) to the C[^]N ligand, which was supported by TD-DFT calculations. All complexes are emissive at 298 K in solid state except **2b** and **3b**, which are only emissive at 77 K having less rigid structure compared to others. The emission of **1a** and **1b** originates from a low-energy excited state of d_{Pt}/π_{SR} → π*_{C[^]N} while **3a** exhibits ³LC/³MLCT transition. For **1a** and **1b**, the radiative rate and the quantum efficiency are higher in rigid environment such as solid compared to polymer and solution. Decreasing the rigidity of environment leads to flexibility of rotation of the –SR around the axis of the Pt–S bond. So the geometry can be easily changed after radiation and the lowest lying triplet excited state would have the effective contribution of dd* transition, which opens a nonradiative pathway at room temperature.

Introduction

Thiolates can act as auxiliary ligands in transition metal complexes (especially in cycloplatinated compounds) and play important roles in the facility of tuning both steric and electronic properties of these complexes.¹⁻⁷ Our recent research revealed that the cyclometalated platinum complexes including thiolate ligands can be an effective target in photophysical studies,⁸⁻¹⁰ fundamental reactions such as C–S bond coupling,¹¹ C–H reductive elimination¹² and protonation reaction¹³ or considered as promising anticancer agents for drug development.¹⁴

However, despite the wide investigation on synthesis of binuclear cycloplatinated complexes containing di- μ -thiolate bridges, which introduced as half-lantern compounds^{12, 15-20} and bidentate platinum complexes containing dithiolate ligands,^{21, 22} examples of mononuclear cyclometalated platinum with a non-bridged thiolate ligand are rare.^{11, 13, 14} The interest for synthesis and photophysical investigation of these kind of complexes comes from the potential of these complexes to efficiently emit in solid state due to the rigidity of some complexes induced by $\pi\cdots\pi$ interactions and a short phosphorescence decay time,⁸⁻¹⁰ since for many technological applications, such as OLED and sensors, the luminescent molecules must be embedded in a solid matrix.^{23, 24} Coupling of strong σ -donating thiolate ligands would make the metal center more electron-rich (according to the electron donor ability of the aromatic ring coordinated to S atom),¹¹ which boosts the luminescence properties of the complexes by raising of the energy of the dd* states, thus increasing the population of the thermally activated excited state.²⁵

As part of our ongoing research into the chemistry of platinum thiolate complexes,¹¹⁻¹⁴ the aim of present work is to introduce a new class of emissive cycloplatinated(II) phosphine complexes with a non-bridging thiolate ligand. Also, the influence of a thiolate ligand on the excited states of the cycloplatinated complexes compared to parent complexes, interpretation of absorption and emission spectra at 298 and 77 K, and the effect of the rigidity of environment are described in detail. For the better understanding of the relationship between structure and photophysical properties, we have employed density functional theory (DFT) and time-dependent DFT (TD-DFT) calculations.

Results and discussion

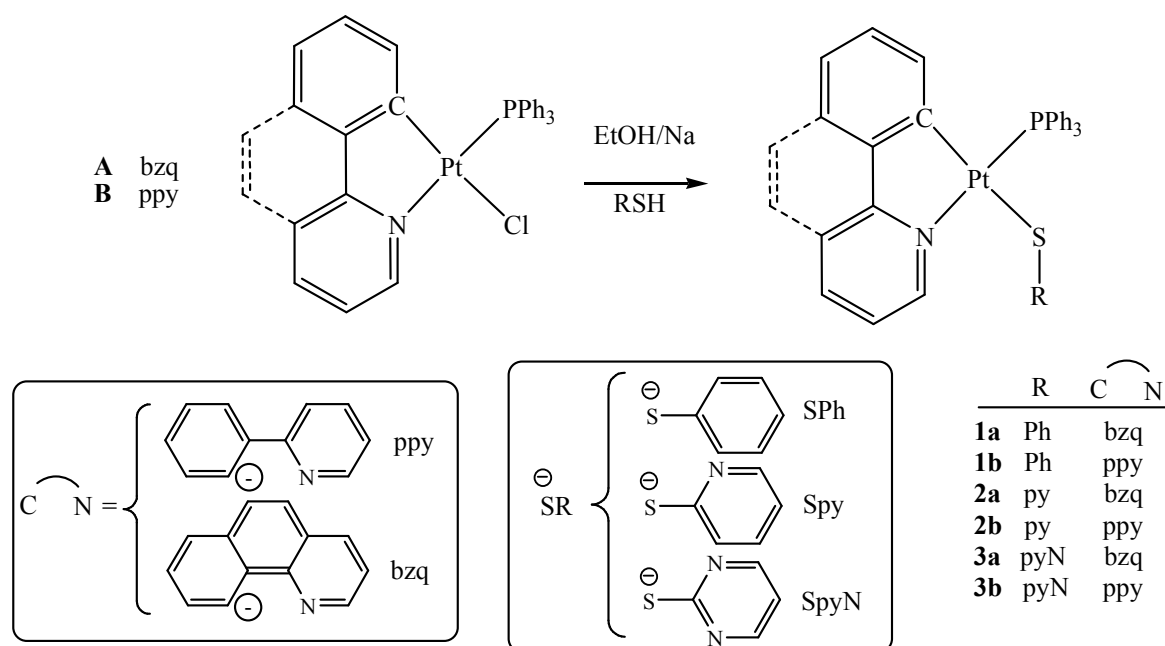
Synthesis and Structural Characterization of Complexes

The new chemistry to prepare cycloplatinated(II) complexes is illustrated in Scheme 1. The reaction of platinum precursor complexes $[\text{Pt}(\text{C}^{\wedge}\text{N})(\text{PPh}_3)\text{Cl}]$, $\text{C}^{\wedge}\text{N} = \text{bzq}$ (7,8-benzoquinoliny, **A**)²⁶ and ppy (2-phenylpyridinyl, **B**),²⁷ with one equivalent of *in situ* freshly prepared sodium thiolate ligands (Na^+SR^-), formed by the reaction of appropriate thiol ligands with sodium metal in ethanol, gave $[\text{Pt}(\text{C}^{\wedge}\text{N})(\text{PPh}_3)(\kappa^1\text{-S-SR})]$, $\text{C}^{\wedge}\text{N} = \text{bzq}$, $\text{R} = \text{SPh}$ (thiophenolate, **1a**); $\text{C}^{\wedge}\text{N} = \text{ppy}$, $\text{R} = \text{SPh}$ (**1b**);¹³ $\text{C}^{\wedge}\text{N} = \text{bzq}$, $\text{R} = \text{Spy}$ (pyridine-2-thiolate, **2a**); $\text{C}^{\wedge}\text{N} = \text{ppy}$, $\text{R} = \text{Spy}$ (**2b**);¹³ $\text{C}^{\wedge}\text{N} = \text{bzq}$, $\text{R} = \text{SpyN}$ (pyrimidine-2-thiolate, **3a**); $\text{C}^{\wedge}\text{N} = \text{ppy}$, $\text{R} = \text{SpyN}$ (**3b**). Complexes **1-3** were deduced from common analytical methods and their formulations were confirmed by good agreement of elemental analyses with calculated values. The integrity of these complexes in solution were characterized by (^1H and $^{31}\text{P}\{^1\text{H}\}$) means of NMR spectroscopy, and schematic labeling is given in Scheme 2. The Experimental Section provides numerical NMR data while the spectra are given in the Supporting Information (Figures S1-S8). Moreover, the solid state structure of **1a** and **2a** were determined by single-crystal X-ray diffraction.

The ^1H NMR spectra of **1-3** display signals for only one kind of cyclometalated, PPh_3 and SPh/Spy/SpyN ligands, corresponding to “ $\text{Pt}(\text{C}^{\wedge}\text{N})(\text{PPh}_3)(\kappa^1\text{-S-SR})$ ” fragments.^{11, 13, 14} Also, the $^{31}\text{P}\{^1\text{H}\}$ NMR spectra of **1-3** show a sharp singlet resonance flanked by platinum satellites, which confirms the coordination of only one phosphine ligand to the platinum center. The large value of the coupling constant between platinum and phosphorus ($^1J_{\text{PtP}} = 4296\text{--}4376$ Hz) confirms a PPh_3 ligand is located in *trans* position of the nitrogen atom of the cyclometalated moiety. Moreover, the other probable isomer ($\text{PPh}_3\text{-trans-C}(\text{sp}^2)$) can be ruled out by regarding to the *transphobia* effect.^{11, 13, 14} This effect has been used to elucidate the stable geometry of square-planar d^8 transition-metal complexes. In these thiolate complexes the PPh_3 ligand contains greater *trans* influence and softer ancillary atom than thiolate ligands is more suitable to locate in *cis* position of Pt–C bond of cyclometalating ligands.^{13, 14}

The structures of **1a**, and **2a** were established by single crystal X-ray analysis, and the structure of **1b** has been reported previously.¹³ Crystallographic data for **1a** and **2a** are collected

in Table S1 and selected bond distances and angles are quoted in Table S2. The perspective drawing of **1a** and **2a** are demonstrated in Figure 1.



Scheme 1. The synthetic route for the formation of **1-3**.

Single crystal X-ray diffraction studies of **1a** and **2a** revealed monomeric four-coordinate distorted square planar structures around the platinum(II) center. The small bite angle of C[^]N chelate ligand (80.84(9) for **1a** and 80.76(9) for **2a**) which caused the distortion from square planar geometry is comparable to other bzq chelate Pt(II) complexes.²⁸⁻³¹ The distances of the Pt–S bonds are almost equal in all complexes (~ 2.36 Å). It is notable that the aromatic ring including the κ¹-S-SR moiety is approximately perpendicular to the metal plane (Figure S9) and the dihedral angle between the metal plane and the aryl ring of thiolate ligand is 82.88° for **1a**, 83.40° for **1b**¹³ and 63.24° for **2a**. Consequently, as is shown in Figure S10, the aromatic ring of the thiolate ligand tends to form intramolecular π···π stacking to one of the phenyl groups of PPh₃ ligand and the distance between two centroids are 3.629 (**1a**), 3.837 (**1b**)¹³ and 3.597 Å (**2a**). Additionally, intermolecular dimer π···π stacking between two bzq groups in **1a** and **2a** (in a head-to-tail fashion) formed supramolecular packing (Figure S10).

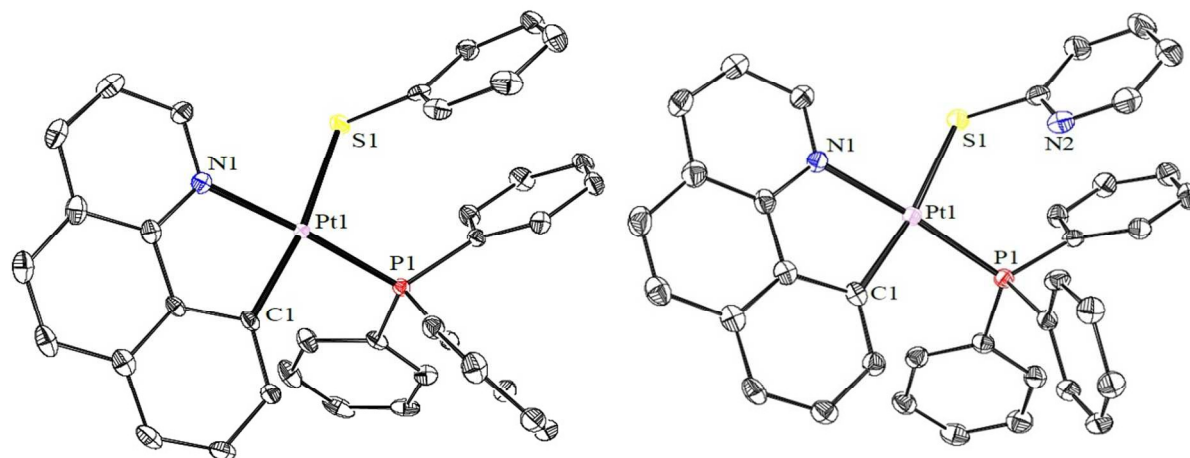


Figure 1. Representations of the X-ray crystal structure of **1a** (left) and **2a** (right). Ellipsoids are drawn at the 40% probability level, and hydrogen atoms and a CH₂Cl₂ solvent molecule in **1a** have been omitted for clarity.

Photophysical properties of complexes

All synthesized complexes are stable in the solid state and solution media. Complexes **1-3** exhibit good solubility in CH₂Cl₂. Photophysical properties of these complexes and precursor complexes (**A** and **B**) were examined by using their absorption and luminescence spectra in solid state, fluid solution (CH₂Cl₂). Complexes **1a** and **1b** were examined in PMMA (poly(methyl methacrylate)) and PS (polystyrene) polymers at 298 and 77 K.

Effect of replacement of Cl by SPh

The replacement of the chloride ligand in **A** or **B** (with green color) by the thiophenolate (SPh) has an observable effect on the absorption spectra, producing final products (**1a** and **1b**) with intense orange color. In Figure 2 (left), the absorption spectrum of **1b** in solid state is shown together with starting chloro complex (**B**). Compounds **1b** and **B** have the same set of intense bands in the UV region ($\lambda < 345$ nm), but some different bands with different molar absorptivity observed in the visible region, causing different color to be observed. The longest-wavelength, spin-allowed broad band in **1b** appears at 502 nm, while in the parent complex (**B**) a well-defined band centered around 478 nm is observed. The appearance of the long-wavelength band in this region related to change of chloride ligand with thiolate ligand can be rationalized in term of a new low-energy charge-transfer state as supported by DFT calculation. In both complexes, the lowest energy excited states arise from HOMO→LUMO transitions. This transition in **B** has

a mixture character attributed to $^1[d_{Pt}/\pi_{Cl}/\pi_{ppy} \rightarrow \pi^*_{ppy}]$ character (Figure 2 (right)). In **1b**, substituting the electron-rich sulfur atom leads to increasing HOMO's energy. This causes a remarkable red shift in lowest energy band with contributing the thiolate and the metal atom in HOMO level, in contrast to the parent chloride complex. Meanwhile, the LUMO can be expected to remain localized largely on the ppy (π^*) ligand. Thus, it can be anticipated the low-energy excited state transition in **1b** has an ascribed mixture character $^1[d_{Pt}/\pi_{SPh} \rightarrow \pi^*_{ppy}]$. The $^1LC_{(ppy)}$ transition is therefore faded, which is supported by TD-DFT calculations (*vide infra*).^{9, 13, 32, 33}

The same trend can be seen in emission spectra. Complex **B** displays vibronically structured bands in the green region ($\lambda = 483$ nm) with a luminescence lifetime of 5.7 μ s, which is proposed as a mixture of $^3LC/^3MLCT$ emission.³⁴ The emission of **1b** is shifted to the red and shows a broad emission ($\lambda_{max} = 577$ nm) with a shorter lifetime of 1.4 μ s in the orange region of the spectrum. This makes clear the profound effect of the substitution of chloride ligand by thiophenolate ligand and changes the character of excited state to $^3[(M+L')LCT]$ ($d_{Pt}/\pi_{SPh} \rightarrow \pi^*_{ppy}$).⁹ The same data were also obtained for **A** and **1a** in both absorption and emission spectra (Table S3 and Table 1).

Absorption Spectra

The absorption spectra of **1-3** in CH_2Cl_2 solution, are shown in Figure 3, and numerical UV-vis data are compiled in Table S3.

In the UV-vis spectra of **1a**, **2a** and **3a** (bzq complexes), two intense high energy absorption bands with large absorption coefficients ($\epsilon > 20000$ $M^{-1}cm^{-1}$) were observed at around $\lambda \leq 300$ nm (Figure 3a) which are attributed to $\pi-\pi^*$ intraligand transitions (1IL) located on the cyclometalated ($L = bzq$), the SR ligand and PPh_3 ligand.³⁵ Electronic transitions with moderate intensity observed at 348 nm ($\epsilon > 6000$ $M^{-1}cm^{-1}$) in **2a** and **3a**, refer to $n-\pi^*$ transition in py and pyN moiety of the thiolate ligands. This assignment is on the basis of the similarity of the absorption bands of the complexes in shape and extinction coefficient compare with absorption bands for HSpY in CH_2Cl_2 solution (at 292 and 375 nm with $\epsilon = 14340$ and 5430 $M^{-1}cm^{-1}$), and two absorption bands (at 282 and 359 nm with $\epsilon = 16060$ and 6390 $M^{-1}cm^{-1}$) for Na^+Spy^- in MeOH solution³⁶ which refer to $\pi-\pi^*$ and $n-\pi^*$ transitions, respectively. However, the absorption spectrum of the thiophenolate complex (**1a**) was characterized by an absorption band

located at 303 nm in CH₃CN ($\epsilon = 13600 \text{ M}^{-1}\text{cm}^{-1}$) as a $\pi\text{-}\pi^*$ transition.³⁷ New low energy bands in **1a**, **2a** and **3a** ($\lambda > 365 \text{ nm}$) in Figure 3a relative to the chloro parent complex (**A**) show new $^1[\text{d}_{\text{Pt}}/\pi_{\text{SR}} \rightarrow \pi^*_{\text{bzq}}]$ transitions.¹³ The order of low energy λ_{max} , SPh > Spy > SpyN is an evidence of contribution of SR ligand in the lowest excited state and is attributed to the effect of the increasingly electron-donating substituent in destabilizing the HOMO which is supported by TD-DFT calculations (Table S4 and Table S5). Figure 3b shows that the spectra of **1b**, **2b** and **3b** (ppy complexes) are similar in shape, but blue-shifted compared to the bzq analogous with decreased absorption coefficients which indicate the existence of a less extended π -conjugated system in ppy complexes.³⁸ Dependency of all excited states on C[^]N ligands are clearer when we compare the spectra of **1a** and **1b** (Figure S11). This dependency on the nature of the C[^]N ligands are due to incorporation of C[^]N ligands in LUMO states (Table S5). Solid state diffuse reflectance UV-vis spectra of the complexes displays a similar pattern to those observed in solution (Figure S12).

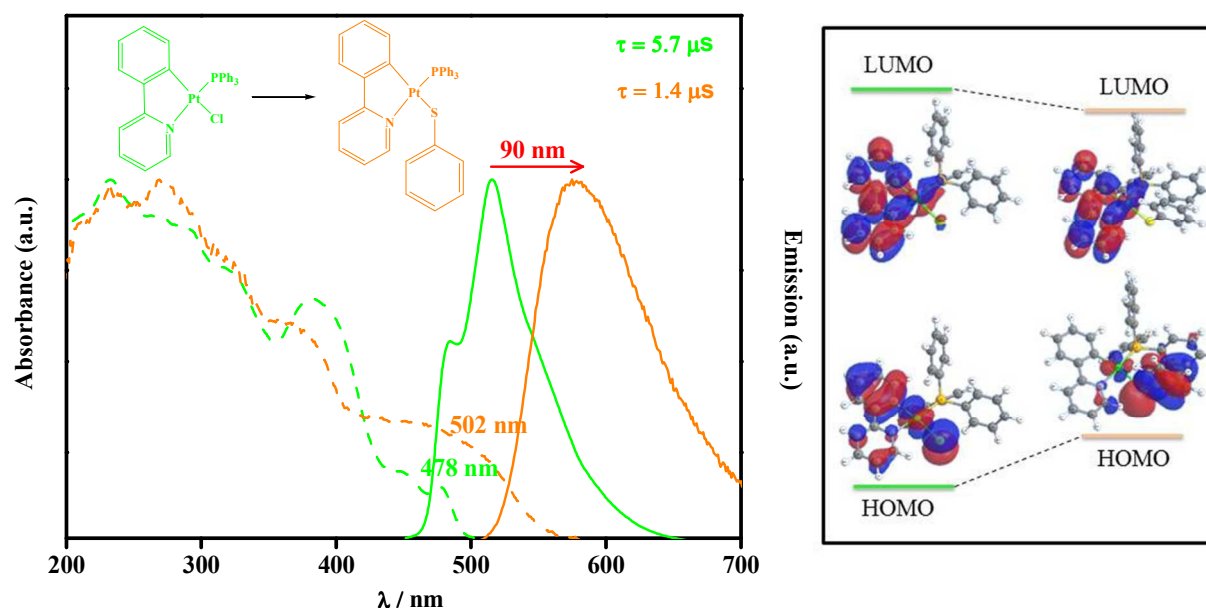


Figure 2. Normalized absorption (dash lines) and emission spectra (solid lines) of **B** (green lines) and **1b** (orange lines) in solid state at 298 K (left). Frontier orbitals of **B** and **1b** calculated by DFT in gas phase (right).

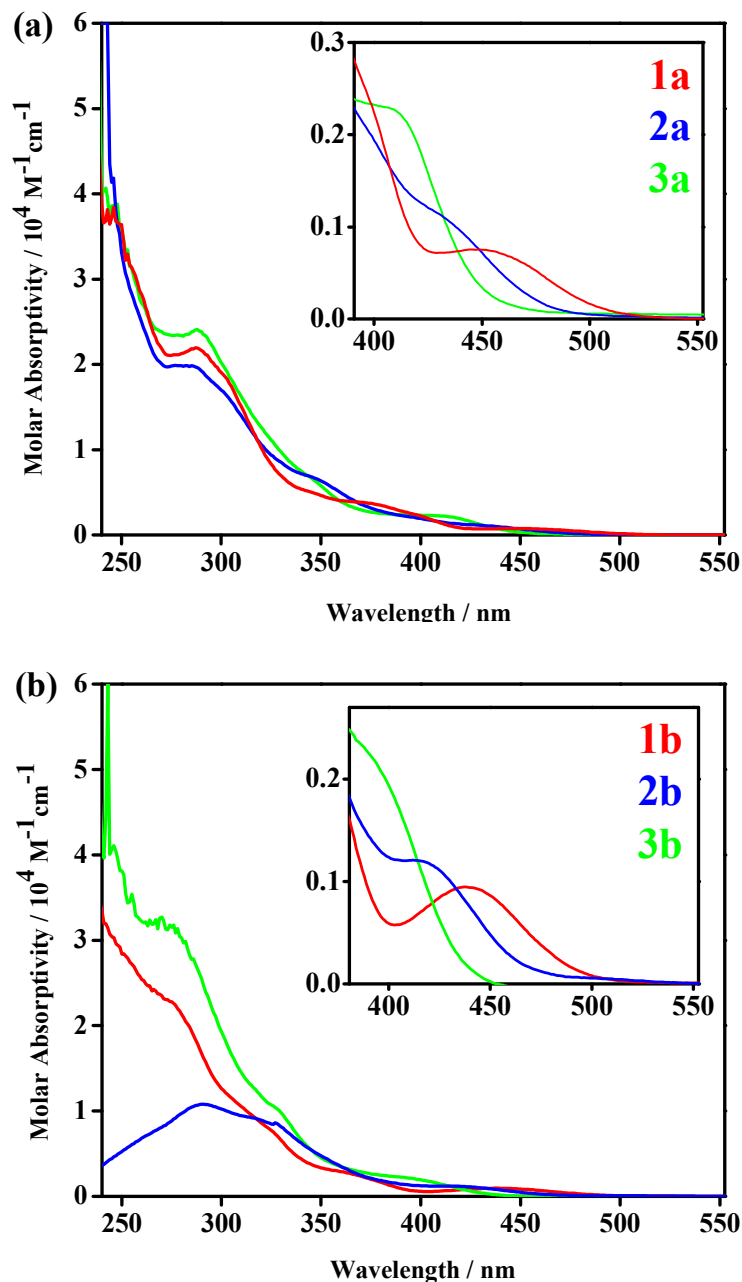


Figure 3. Absorption spectra of (a) **1a**, **2a** and **3a**; (b) **1b**, **2b** and **3b** in CH₂Cl₂ at 298 K (the insets show the expansion of the region of the low-energy bands).

Emission Spectra

Table 1 provides a summary of the emission maxima (λ_{max}), lifetimes (τ), and photoluminescence quantum yields (Φ_{PL}) of complexes. Excitation and emission spectra of **1a**, **2a**, **3a** and **1b** at 298 K in the solid state are presented in Figure 4.

Table 1. Emission data for **A**, **B**, **1-3**.

Comp.	Media	Temp.	λ_{em} [nm]	τ_{em} (μ s) ^b	Φ_{PL} ^b [%]	$k_r = \Phi/\tau$ [s^{-1}]	k_{nr} [s^{-1}]
A	Solid	298 K	480, 508, 578	3.96	3	7.6×10^3	6.2×10^4
B	Solid	298 K	483, 516 _{max} , 560 _{sh}	5.7	5	6.2×10^4	1.2×10^6
1a	Solid	298 K	572	1.27	43	3.4×10^5	4.5×10^5
		77 K	570	5.86	79	1.3×10^5	3.6×10^4
	PMMA	298 K	584	1.61	4	2.5×10^4	6.0×10^5
		77 K	564	13.54	≈ 100	7.4×10^4	-
	PS	298 K	583	1.45	11	7.6×10^4	6.1×10^5
1b	Solid	298 K	577	1.43	36	2.5×10^5	4.5×10^5
		77 K	575, 602 _{sh}	6.91	95	1.4×10^5	7.2×10^3
	PMMA	298 K	565	1.70	3	1.8×10^4	5.7×10^5
	PS	298 K	566	2.10	12	5.7×10^4	4.2×10^5
		77 K	550	9.24	98	1.1×10^5	2.2×10^3
2a	Solid	298 K	512	0.69	22	3.2×10^5	11.1×10^5
		77 K	513	9.50	98	1.0×10^5	2.1×10^3
3a	Solid	298 K	474 _{max} , 504, 540 _{sh}	0.55	3	5.4×10^4	16.6×10^5
		77 K	510 _{max} , 534, 575 _{sh}	11.22	37	3.3×10^4	5.6×10^4
2b ^a	Solid	77 K	534 _{max} , 554	6.00	-	-	-
3b ^a	Solid	77 K	541	8.55	-	-	-

^aComplexes **2b** and **3b** are not emissive at 298 K. ^bLifetime and quantum yield were measured in neat powder or polymer film.

At ambient temperature (see Figure 4), **2a** shows unstructured green emission and **3a** shows vibronic blue-green emission, whilst, **1a** and **1b** exhibit broad efficient orange emission with peak maxima at 577 nm and 572 nm, respectively.

In a series of bzq complexes, **1a**, **2a** and **3a**: a) the emission maxima are red-shifted in the λ_{max} order SpyN (**3a**, 474 nm) < Spy (**2a**, 512 nm) < SPh (**1a**, 572 nm) which are in agreement with the theoretical wavelengths of the lowest lying triplet excited states (Table S4). b) The long decay time which is indicative of phosphorescence emission increases from 0.55 μ s in **3a** (SpyN) to 0.69 μ s in **2a** (Spy) and 1.27 μ s in **1a** (SPh). c) The quantum yields follow the same trend as

decay times (SPh (43%) > Spy (22%) > SpyN (3%)) which confirm the same trend in radiative rate constants in these complexes.

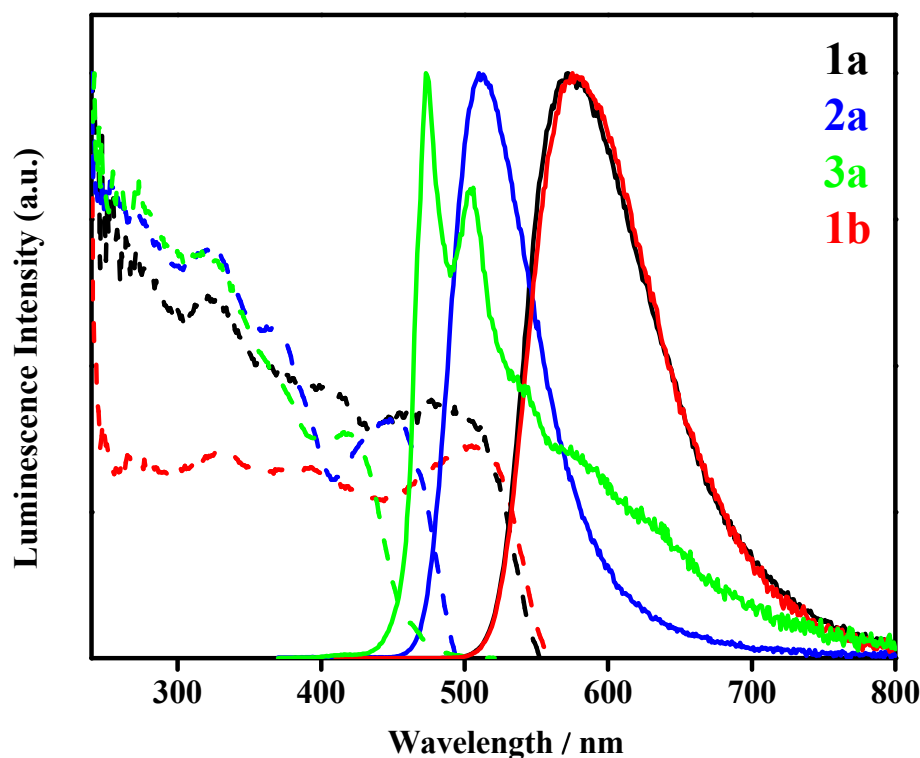


Figure 4. Normalized excitation (dash lines) and emission (solid lines) spectra of the complexes in the solid state at 298 K.

The emission spectrum of **1b** is approximately identical with that of **1a** which proposed a common excited state for both complexes and higher decay times compare to other complexes. Unlike literature reports,^{29, 38} **1a** with higher π conjugated ligand (bzq) shows 5 nm blue shift compared to **1b**. This small shift (found also in the precursors **A** and **B**) suggests the influence of intramolecular $\pi \cdots \pi$ interactions between in which induces red shift on ^1IL and $^1\text{MLCT}$ transitions in absorption spectra, but blue-shift of $^3\text{MLCT}$ excited state in the emission spectra.³⁹ It is noteworthy that in less rigid and diluted media such as polymers (where no such interactions is expected), the opposite trend occurs (see Table 1).

In **3a**, the vibronic structured emission band together with the similarity of emission to the emission of parent complex (**A**) exhibit the phosphorescence from mixture of ^3LC (ligand

centered, $\pi \rightarrow \pi^*$ (bzq))³MLCT (metal to ligand charge transfer, Pt \rightarrow bzq) and negligible effective of SpyN ligand in the excited state.

Complexes **2b** and **3b** are not emissive at room temperature. According to DFT calculations of optimized geometries in ground (S_0) and excited states (T_1) shown in Figures 5 and S13, the geometries of **2b** and **3b** undergo a large distortion from square planar in S_0 geometry to distorted tetrahedral geometry in the triplet geometry, (the R group of SR ligands position parallel to ppy ligand). As a result, the contribution of MC (dd^*) character in the lowest lying excited states (originates from transition between HSOMO and LSOMO) shows a considerable increase, which opens a nonradiative deactivation pathway at 298 K.

According to experimental results, we assumed that the geometry change is negligible in other emissive complexes in rigid matrixes due to $\pi \cdots \pi$ interaction between the R group of SR and one phenyl group of PPh₃ ligand causes less flexibility. Thus, to understand the character of emission of these complexes in the absence of probable thermally activated pathways, we restricted the geometry change of these complexes and calculated lowest lying triplet excited states. The results show that the first triplet excited states originate from transition between HSOMO and LSOMO where HSOMO and LSOMO have the same character as LUMO and HOMO, respectively (Figure 6). As supported by TD-DFT calculations, a low-energy excited state of $d_{Pt}/\pi_{SR} \rightarrow \pi^*_{C^N}$ character may thus be anticipated.

Upon cooling to 77 K, the decay times increase to 5-12 μ s by decrease of nonradiative rate constants. For **1a**, **1b**, and **2a**, the emission spectra at 77 K are close to those at 298 K (Figure 7a). Lack of a clear vibronic structure even at 77 K in these complexes, suggests that the emission is unlikely to be originated from ³LC transition and a low-energy excited state of $d_{Pt}/\pi_{SR} \rightarrow \pi^*_{C^N}$ character may thus be anticipated.

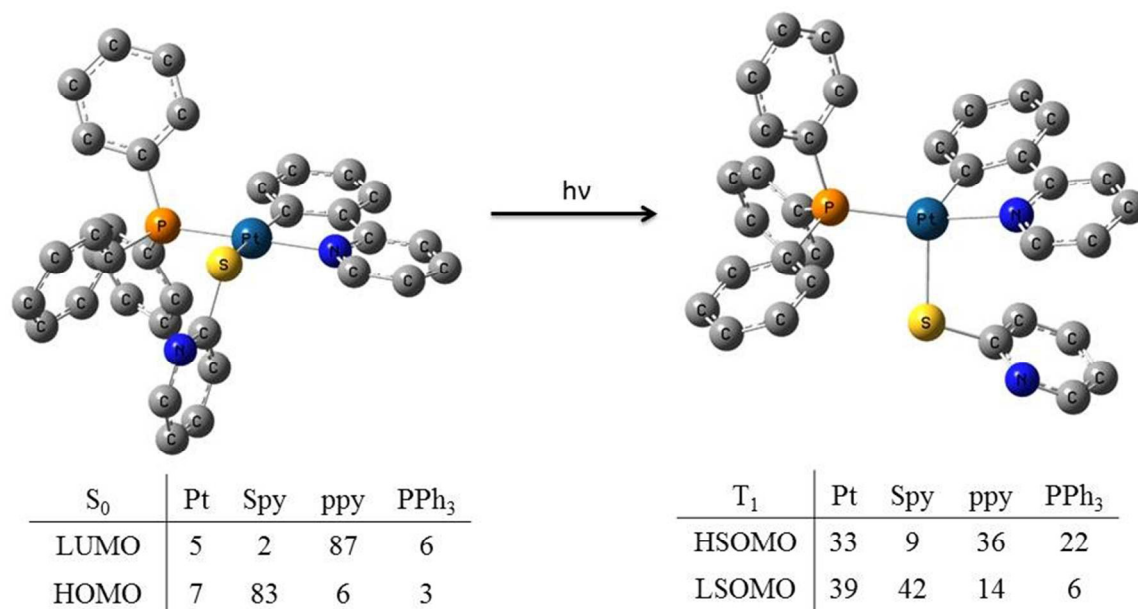


Figure 5. DFT optimized S_0 (left) and T_1 (right) geometries of **2b** with corresponding contribution of different fragments in frontier molecular orbitals obtained in S_0 and T_1 states (H atoms are omitted for clarity of presentation).

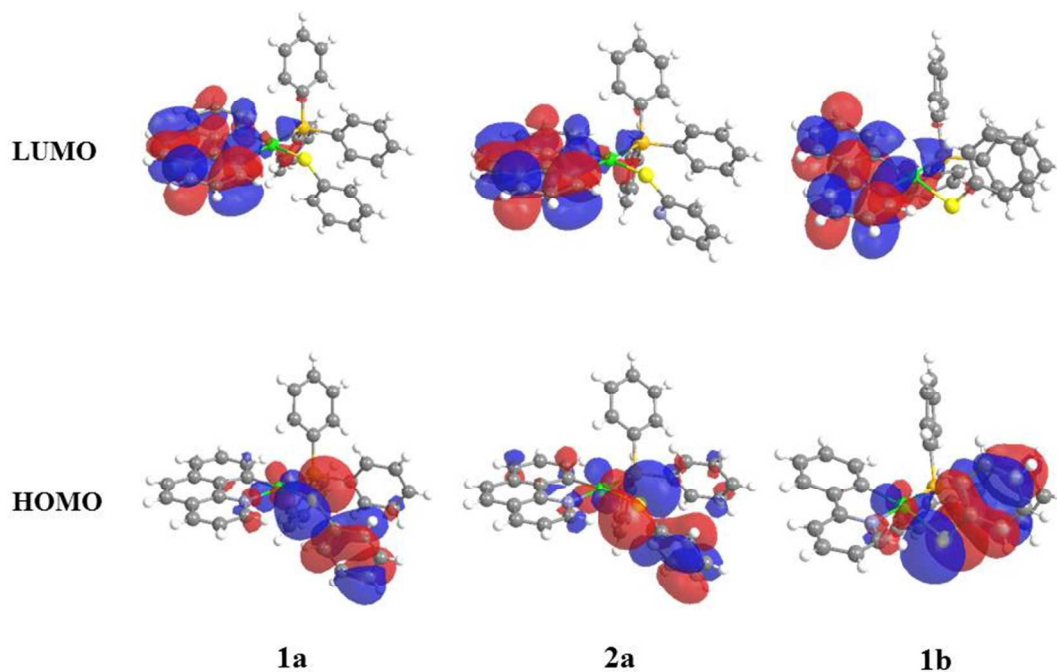


Figure 6. Frontier orbitals of complexes **1a**, **2a**, and **1b** which are responsible for the first triplet excited state in gas phase.

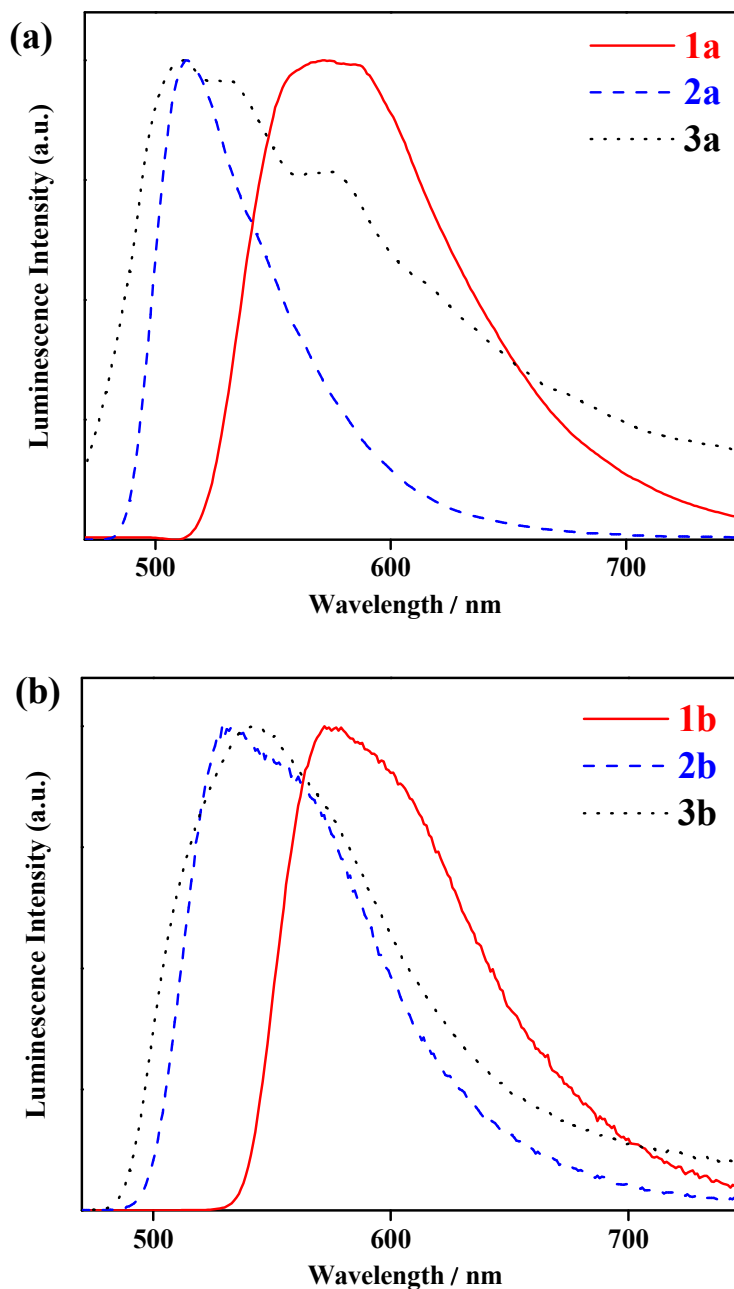


Figure 7. Normalized emission spectra of the complexes (a) **1a**, **2a** and **3a**; (b) **1b**, **2b** and **3b** in the solid state at 77 K.

Compounds **2b** and **3b** show emission bands at λ_{\max} 534 and 541 nm at 77 K, respectively (Figure 7b), where the thermally activated population of the MC states cannot occur due to the limitation of geometry change compared to room temperature. All thiolate complexes are not emissive in solution at 298 K, because the emission properties are crucially determined by the different molecular rigidities of the compounds. Studied complexes can easily undergo

geometrical distortions upon excitation such as torsional distortions away from square planarity to a tetrahedral symmetry in non rigid environment. This can lead to a stabilization of the dd^* state(s) and increasing of their thermal population. However, in a more “rigid” environment, such distortions that lead to related energy stabilizations of the quenching states are less distinct.⁴⁰

Effect of rigidity on emission efficiency

To investigate the influence of rigidity of environment on emission properties of complexes which effects on the different interactions, measurement of emission of **1a** and **1b** has been done in PS and PMMA films (Figure S14). Quantum yield of **1a** decreases in the order of solid (43%) > PS Film (11%) > PMMA Film (4%). The same trend is seen for complex **1b**, solid (36%) > PS (12%) > PMMA (3%). The decrease of Φ_{PL} in comparison to solid state in these complexes is accompanied by a slight increase of the emission lifetime in PS and PMMA matrixes, respectively. These features afford in the polymer matrixes, a decrease of about one order of magnitude of the radiative rate constant. Three main factors for interpreting the more quantum efficiency in a high rigid environment such as solid are listed below: (1) in a rigid media, complexes benefit from the restriction of the vibrational motions responsible for nonradiative decay. (2) Additionally, intermolecular $\pi \cdots \pi$ stacking operating in solid state can lead to more emissive excited states.²³ (3) Besides, intramolecular $\pi \cdots \pi$ stacking between phenyl groups of PPh₃ and SPh ligands limits flexibility of rotation of the –SPh containing aryl ring about the axis of the Pt–S bond, which causes geometry change in the excited state as mentioned before.

Although the emission efficiency for other complexes in polymer films and solution were negligible, heterocyclic thiol derivatives such as Spy and SpyN molecules have distinct properties that can be remarkably different from those displayed by the normal aromatic thiols such as thiophenol.⁴¹ So the uncoordinated nitrogen atom in pyridyl or pyrimidin may interact rapidly and reversibly with available protons in the polymer or solvent and quench the emission.³

Conclusion

The present study extends the information on the structures and optical properties of cyclometalated platinum(II) complexes containing thiolate ligands. We have reported the synthesis of cycloplatinated thiolate complexes (**1-3**) by the salt metathesis reaction on the corresponding chloro precursor complexes (**A** and **B**) with *in situ* prepared Na^+SR^- . This reaction changes the lowest-energy singlet and triplet excited states, to ones that feature charge transfer from the thiolate (mixed with some metal character) to the $\text{C}^{\wedge}\text{N}$ ligand. This is supported by TD-DFT calculations and by the observation that the decreasing energies of the bands correlate with the electron-donating ability of the thiolate.

All complexes are emissive at ambient temperature in solid state with the exception of **2b** and **3b**, which are only emissive at low temperature. Emission spectra of **1a** and **1b** are approximately identical and originate from a low-energy excited state of $d_{\text{Pt}}/\pi_{\text{SR}} \rightarrow \pi^*_{\text{C}^{\wedge}\text{N}}$. Complex **3a** exhibits the phosphorescence from mixture of $^3\text{LC} (\pi \rightarrow \pi^* (\text{bzq})) / ^3\text{MLCT} (\text{Pt} \rightarrow \text{bzq})$.

Upon excitation studied complexes can easily undergo geometrical distortions from square planar to a distorted tetrahedral geometry in non rigid environment. This can lead to a stabilization of the dd^* state(s) and increasing the contribution of MC (dd^*) character in the lowest lying excited states increase which opens a nonradiative deactivation pathway at 298 K.

Experimental

General procedures and materials

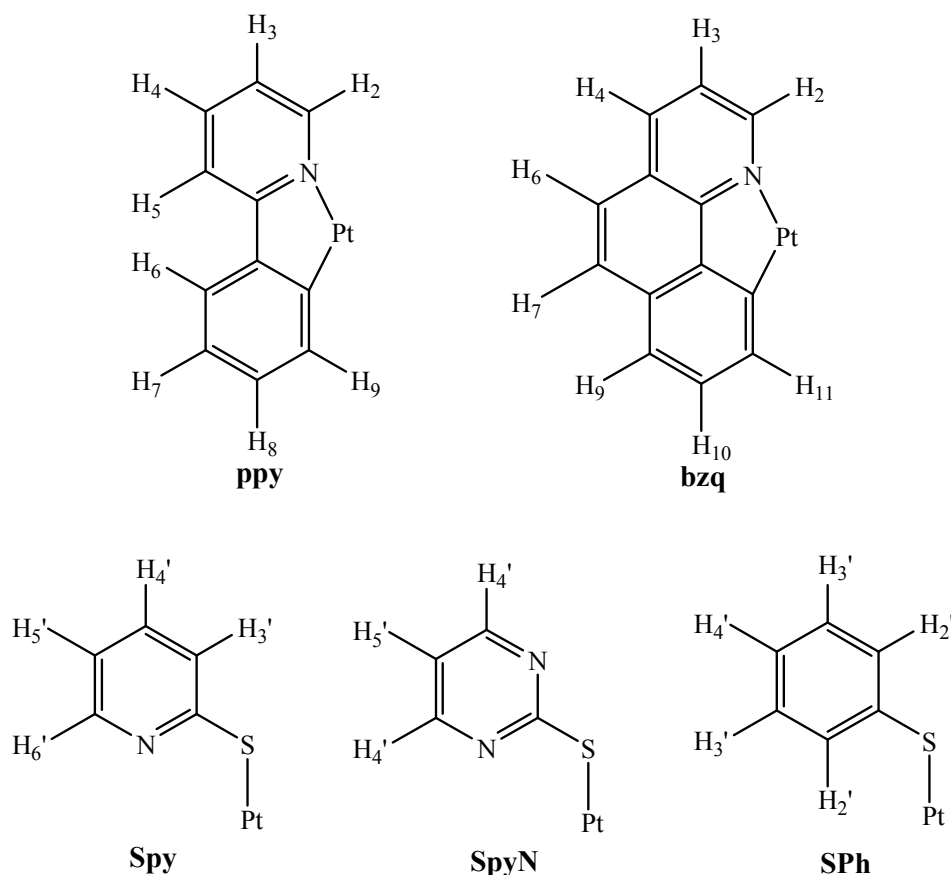
All the reactions were carried out in the common solvents and all solvents were purified and dried according to standard procedures.⁴² The microanalyses were performed using a vario EL CHNS elemental analyzer and also all the melting point values were measured by a Buchi 510. Multinuclear (^1H , and $^{31}\text{P}\{\text{H}\}$) NMR spectra were recorded on a Bruker Avance DPX 400 MHz spectrometer at 293 K. All chemical shifts are reported in ppm (part per million) relative to their corresponding external standards (SiMe_4 for ^1H and 85% H_3PO_4 for $^{31}\text{P}\{\text{H}\}$) and all the coupling constants (J values) are given in Hz. The UV-vis absorption spectra were carried out in a PerkinElmer Lambda 25 spectrophotometer in a cuvette with a 1 cm and/or 1 mm path length. Diffuse reflectance UV-vis (DRUV) data of the pressed powders were recorded on UV/VIS/NIR

spectrometer Cary 5-E (Varian). Luminescence spectra were measured with a Horiba Jobin Yvon Fluorolog 3 steady-state fluorescence spectrometer. For decay time measurements, a PicoQuant FB-375 pulsed diode laser ($\lambda_{\text{exc}} = 378$ nm, pulse width 100 ps) was applied as the excitation source. The emission signal was detected with a cooled photomultiplier attached to a FAST ComTec multichannel scalar card with a time resolution of 250 ps. Absolute measurements of the photoluminescence quantum yield at ambient temperature under Ar and at 77 K were performed with a C9920-02 (Hamamatsu Photonics) system equipped with a Spectralon® integrating sphere. Polymer films containing about 0.1 weight% of the Pt complexes were obtained by dissolving the emitter and polymer in dichloromethane and spin-coating the solutions onto quartz glass substrates. Poly(methyl methacrylate) (PMMA) and polystyrene (PS) films were measured under continuous flushing with nitrogen. 7,8-Benzoquinoline (Hbzq), 2-phenylpyridine (Hppy), thiophenol (HSPh), pyridine-2-thiol (HSpy) and pyrimidine-2-thiol (HSpyn) were purchased from Aldrich or Acros. Complexes [Pt(bzq)(PPh₃)Cl], **A**,²⁶ [Pt(ppy)(PPh₃)Cl], **B**,²⁷ [Pt(ppy)(PPh₃)(κ^1 -S-SPh)], **1b**,¹³ [Pt(ppy)(PPh₃)(κ^1 -S-Spy)], **2b**,¹³ were prepared as reported in literature. The NMR labeling for the ligands are shown in Scheme 2 for clarifying the chemical shift assignments. Additional data for **A**: ¹H NMR (400 MHz, CD₂Cl₂, 20 °C, δ): 10.01 (ddd, ³J_{HH} = 4.7, ⁴J_{PH} = 1.4, 1H, H²), 8.42 (dd, ³J_{HH} = 8.0, ⁴J_{HH} = 1.3, 1H, H⁴), 7.87-7.79 (m, 6H, H^o of PPh₃), 7.78 (d, ³J_{HH} = 8.7, 1H, H⁶), 7.70 (ddd, ³J_{HH} = 5.4, ⁵J_{PH} = 1.5, 1H, H³), 7.66 (d, ³J_{HH} = 8.7, 1H, H⁷), 7.51-7.44 (m, 4H, H⁹ and H^p of PPh₃), 7.43-7.36 (m, 6H, H^m of PPh₃), 6.91 (m, ³J_{PH} = not resolved, 1H, H¹¹), 6.82 (ddd, ³J_{HH} = 3.0 and 3.1, ⁵J_{PH} = 0.8, 1H, H¹⁰); ³¹P {¹H} NMR (162 MHz, CD₂Cl₂, 20 °C, δ): 22.51 (s, ¹J_{PT} = 4329, 1P).

[Pt(bzq)(PPh₃)(κ^1 -S-SPh)], **1a**.

Complex **A** (100 mg, 0.15 mmol) was added to an ethanolic solution of sodium thiophenol ligand (NaC₆H₅S) under inert atmosphere condition [NaC₆H₅S prepared by dissolving of sodium (4.6 mg, 0.20 mmol) in 10 mL of absolute ethanol and was treated with thiophenol (15.2 μ L, 0.15 mmol)]. Orange solution was formed and after stirring for 5 h at room temperature a yellow-orange solid precipitated which was separated, washed with ethanol (3 \times 2 mL) and cold acetone (2 \times 2 mL) and dried yielding complex **1a**. Yield: 67 mg, 61%; m.p = 240 °C. Anal. Calcd for C₃₇H₂₈NPPtS (744.74): C, 59.67; H, 3.79; N, 1.88; Found: C, 59.42; H, 3.72; N, 1.92. ¹H NMR (400 MHz, dms_o-*d*₆, 20 °C) δ : 10.06 (m, ³J_{PH} = not resolved, 1H, H²), 8.67 (d, ³J_{HH} =

8.0, 1H, H⁴), 7.90 (d, ³J_{HH} = 8.7, 1H, H⁶), 7.83 (d, ³J_{HH} = 8.7, 1H, H⁷), 7.77 (t, ³J_{HH} = 6.4, 1H, H³), 7.73-7.64 (m, 6H, H^o of PPh₃), 7.58 (d, ³J_{HH} = 7.8, 1H, H⁹), 7.49-7.41 (m, 3H, H^p of PPh₃), 7.41-7.32 (m, 6H, H^m of PPh₃), 7.18 (d, ³J_{HH} = 7.7, 2H, H^{2'}), 6.99 (t, ³J_{HH} = 7.6, 1H, H¹⁰), 6.83 (dd, ³J_{HH} = 7.4, ⁴J_{PH} = 2.5, ³J_{PtH} = not resolved, 1H, H¹¹), 6.76-6.69 (m, 2H, H^{3'}), 6.65 (t, ³J_{HH} = 7.2, 1H, H^{4'}); ³¹P{¹H} NMR (162 MHz, dms_o-d₆, 20 °C) δ: 23.02 (s, ¹J_{PtP} = 4296, 1P).



Scheme 2. Numerical Scheme for ¹H NMR assignment.

The following complexes were made similarly using the appropriate precursor complexes and ligands.

[Pt(bzq)(PPh₃)(κ¹-S-Spy)], 2a.

Yield: 104 mg, 67%; m.p = 256 °C. Anal. Calcd for C₃₆H₂₇N₂P₂S (745.73): C, 57.98; H, 3.65; N, 3.76; Found: C, 57.94; H, 3.66; N, 3.87. ¹H NMR (400 MHz, dms_o-d₆, 20 °C) δ: 10.00 (m, ³J_{PtH} = not resolved, 1H, H²), 8.70 (dd, ³J_{HH} = 8.1, ⁴J_{HH} = 1.2, 1H, H⁴), 7.92-7.79 (m, 4H, H⁶, H⁷, H³ and H^{6'}), 7.76-7.67 (m, 6H, H^o of PPh₃), 7.57 (d, ³J_{HH} = 7.8, 1H, H⁹), 7.46-7.40 (m, 3H, H^p of

PPh₃), 7.39-7.31 (m, 6H, H^m of PPh₃), 7.01-7.95 (m, 2H, H¹⁰ and H^{3'}), 6.92 (td, ³J_{HH} = 7.6, ⁴J_{HH} = 1.9, 1H, H^{4'}), 6.81 (dd, ³J_{HH} = 7.6, ⁴J_{PH} = 2.4, ³J_{PH} = 38.1, 1H, H¹¹), 6.58 (ddd, ³J_{HH} = 4.9, ⁴J_{HH} = 1.1, 1H, H^{5'}); ³¹P{¹H} NMR (162 MHz, dms_o-d₆, 20 °C) δ: 22.10 (s, ¹J_{PtP} = 4342, 1P).

[Pt(bzq)(PPh₃)(κ¹-S-SpyN)], **3a**.

Yield: 64 mg, 58%; m.p = 281 °C. Anal. Calcd for C₃₅H₂₆N₃PPtS (746.72): C, 56.30; H, 3.51; N, 5.63; Found: C, 56.24; H, 3.58; N, 5.56. ¹H NMR (400 MHz, dms_o-d₆, 20 °C) δ: 10.10 (m, ³J_{PH} = not resolved, 1H, H²), 8.72 (d, ³J_{HH} = 7.8, 1H, H⁴), 7.97 (d, ³J_{HH} = 4.7, 2H, H^{4'}), 7.92-7.82 (m, 3H, H⁶, H⁷, H³), 7.77-7.68 (m, 6H, H^o of PPh₃), 7.56 (d, ³J_{HH} = 8.0, 1H, H⁹), 7.45-7.384 (m, 3H, H^p of PPh₃), 7.378-7.30 (m, 6H, H^m of PPh₃), 6.96 (t, ³J_{HH} = 7.5, 1H, H¹⁰), 6.81 (ddd, ³J_{HH} = 7.3, ⁴J_{PH} = 2.8, ⁴J_{HH} = 0.7, ³J_{PH} = not resolved, 1H, H¹¹), 6.66 (t, ³J_{HH} = 4.8, 1H, H^{5'}); ³¹P{¹H} NMR (162 MHz, dms_o-d₆, 20 °C) δ: 21.48 (s, ¹J_{PtP} = 4376, 1P).

[Pt(ppy)(PPh₃)(κ¹-S-SpyN)], **3b**.

Yield: 60 mg, 54%; m.p = 263 °C. Anal. Calcd for C₃₃H₂₆N₃PPtS (722.70): C, 54.84; H, 3.63; N, 5.81; Found: C, 54.91; H, 3.56; N, 5.76. ¹H NMR (400 MHz, dms_o-d₆, 20 °C) δ: 9.83 (m, ³J_{PH} = not resolved, 1H, H²), 8.18 (d, ³J_{HH} = 7.8, 1H, H⁵), 8.10 (t, ³J_{HH} = 7.8, 1H, H⁴), 7.98 (d, ³J_{HH} = 4.7, 2H, H^{4'}), 7.80 (d, ³J_{HH} = 7.8, 1H, H⁶), 7.73-7.64 (m, 6H, H^o of PPh₃), 7.50-7.29 (m, 10H, H³, H^p and H^m of PPh₃), 6.96 (t, ³J_{HH} = 7.5, 1H, H⁷), 6.66 (t, ³J_{HH} = 4.8, 1H, H⁸), 6.63 (m, ³J_{PH} = not resolved, 1H, H⁹), 6.52 (t, ³J_{HH} = 7.2, 1H, H^{5'}); ³¹P{¹H} NMR (162 MHz, dms_o-d₆, 20 °C) δ: 22.27 (s, ¹J_{PtP} = 4364, 1P).

Crystal Structure Determination and Refinement

Diffraction data were collected on a SuperNova X-ray diffraction system equipped with a CuK_α radiation source (λ = 1.54184 Å). The data were collected at 123 K using an Oxford Instruments Cryojet Cooler for **2a** or at 294 K for **1a**. The structures were solved by Intrinsic Phasing using the ShelXT (Sheldrick, 2015) structure solution program⁴³ and refined by Least Squares using version 2014/7 of ShelXL (Sheldrick, 2015).⁴⁴ All non-hydrogen atoms were refined anisotropically. Hydrogen atom positions were calculated geometrically and refined using the riding model. Details of crystal and structure refinement are listed in Table S1.

Computational methods

The DFT optimized S_0 and T_1 geometries of all complexes were calculated theoretically at the B3LYP/6-31G(d) level (LANL2DZ for Pt). TD-DFT calculations on the optimized ground state singlet geometries were performed to gain insight in nature of singlet transitions of the complexes besides the experimental observations.⁴⁵ In order to estimate the phosphorescence wavelengths, TD-DFT computations were done on X-ray structure of complexes. Percentages compositions of molecular orbitals and theoretical absorption spectra were plotted using Chemissian program.⁴⁶

Electronic supplementary information (ESI) available: NMR spectra, crystallographic and computational details. Crystallographic data (excluding structure factors) for the structural analysis has been deposited with the Cambridge Crystallographic Data Centre, No. CCDC-1547213 (**1a**), CCDC-1547214 (**2a**).

Acknowledgments

This work was supported by the Institute for Advanced Studies in Basic Sciences (IASBS) Research Council, Shiraz University and the Iran National Science Foundation (Grant no. 95834232). M. Jamshidi gratefully acknowledges Professor Hartmut Yersin for valuable discussions and guidance and providing facilities during her sabbatical leave at Regensburg University. She also thanks MSRT for financial support. Thanks, are also due to Mr. A. Biglari, the operator of Bruker NMR instrument at IASBS, for recording the NMR spectra.

References:

1. T. Fischer, R. Czerwieniec, T. Hofbeck, M. M. Osminina and H. Yersin, *Chem. Phys. Lett.*, 2010, **486**, 53-59.
2. W. Paw, S. D. Cummings, M. A. Mansour, W. B. Connick, D. K. Geiger and R. Eisenberg, *Coord. Chem. Rev.*, 1998, **171**, 125-150.
3. W. Paw, R. J. Lachicotte and R. Eisenberg, *Inorg. Chem.*, 1998, **37**, 4139-4141.
4. E. S. Raper, *Coord. Chem. Rev.*, 1985, **61**, 115-184.
5. E. S. Raper, *Coord. Chem. Rev.*, 1996, **153**, 199-255.

6. E. S. Raper, *Coord. Chem. Rev.*, 1997, **165**, 475-567.
7. V. Cordero-Pensado, V. Gómez-Benítez, S. Hernández-Ortega, R. A. Toscano and D. Morales-Morales, *Inorg. Chim. Acta*, 2006, **359**, 4007-4018.
8. J. R. Berenguer, E. Lalinde, A. Martín, M. T. Moreno, S. Ruiz, S. Sánchez and H. R. Shahsavari, *Inorg. Chem.*, 2014, **53**, 8770-8785.
9. J. R. Berenguer, E. Lalinde, A. Martín, M. T. Moreno, S. Sánchez and H. R. Shahsavari, *Inorg. Chem.*, 2016, **55**, 7866-7878.
10. J. R. Berenguer, E. Lalinde, A. Martín, M. T. Moreno, S. Ruiz, S. Sanchez and H. R. Shahsavari, *Chem. Commun.*, 2013, **49**, 5067-5069.
11. M. Niazi, H. R. Shahsavari, M. Golbon Haghghi, M. R. Halvagar, S. Hatami and B. Notash, *RSC Adv.*, 2016, **6**, 95073-95084.
12. M. Dadkhah Aseman, S. M. Nabavizadeh, H. R. Shahsavari and M. Rashidi, *RSC Adv.*, 2015, **5**, 22692-22702.
13. M. Niazi, H. R. Shahsavari, M. Golbon Haghghi, M. R. Halvagar, S. Hatami and B. Notash, *RSC Adv.*, 2016, **6**, 76463-76472.
14. M. Fereidoonzhad, M. Niazi, Z. Ahmadipour, T. Mirzaee, Z. Faghieh, Z. Faghieh and H. R. Shahsavari, *Eur. J. Inorg. Chem.*, 2017, 2247-2254.
15. V. Sicilia, M. Baya, P. Borja and A. Martín, *Inorg. Chem.*, 2015, **54**, 7316-7324.
16. V. Sicilia, P. Borja, J. M. Casas, S. Fuertes and A. Martín, *J. Organomet. Chem.*, 2013, **731**, 10-17.
17. V. Sicilia, P. Borja and A. Martín, *Inorganics*, 2014, **2**, 508.
18. R. Aoki, A. Kobayashi, H.-C. Chang and M. Kato, *Bull. Chem. Soc. Jpn.*, 2011, **84**, 218-225.
19. V. Sicilia, P. Borja, M. Baya and J. M. Casas, *Dalton Trans.*, 2015, **44**, 6936-6943.
20. T. Koshiyama, A. Omura and M. Kato, *Chem. Lett.*, 2004, **33**, 1386-1387.
21. J. Moussa, L. M. Chamoreau, M. P. Gullo, A. Degli Esposti, A. Barbieri and H. Amouri, *Dalton Trans.*, 2016, **45**, 2906-2913.
22. H. Sesolis, J. Moussa, G. Gontard, A. Jutand, M. P. Gullo, A. Barbieri and H. Amouri, *Dalton Trans.*, 2015, **44**, 2973-2977.
23. M. Panigati, M. Mauro, D. Donghi, P. Mercandelli, P. Mussini, L. De Cola and G. D'Alfonso, *Coord. Chem. Rev.*, 2012, **256**, 1621-1643.

24. H. Yersin, in *Highly Efficient OLEDs with Phosphorescent Materials*, Wiley-VCH Verlag GmbH & Co. KGaA, 2007.
25. V. W.-W. Yam and K. M.-C. Wong, *Chem. Commun.*, 2011, **47**, 11579-11592.
26. P. S. Pregosin, F. Wombacher, A. Albinati and F. Lianza, *J. Organomet. Chem.*, 1991, **418**, 249-267.
27. H. Samouei, M. Rashidi and F. W. Heinemann, *J. Iran. Chem. Soc.*, 2014, **11**, 1207-1216.
28. M. Fereidoonzhad, B. Kaboudin, T. Mirzaee, R. Babadi Aghakhanpour, M. Golbon Haghighi, Z. Faghieh, Z. Faghieh, Z. Ahmadipour, B. Notash and H. R. Shahsavari, *Organometallics*, 2017, **36**, 1707-1717.
29. M. Jamshidi, S. M. Nabavizadeh, H. Sepehrpour, F. Niroomand Hosseini, R. Kia and M. Rashidi, *J. Lumin.*, 2016, **179**, 222-229.
30. S. M. Nabavizadeh, M. Golbon Haghighi, A. R. Esmaeilbeig, F. Raouf, Z. Mandegani, S. Jamali, M. Rashidi and R. J. Puddephatt, *Organometallics*, 2010, **29**, 4893-4899.
31. A. Bossi, A. F. Rausch, M. J. Leitzl, R. Czerwieniec, M. T. Whited, P. I. Djurovich, H. Yersin and M. E. Thompson, *Inorg. Chem.*, 2013, **52**, 12403-12415.
32. W. A. Tarran, G. R. Freeman, L. Murphy, A. M. Benham, R. Katakya and J. G. Williams, *Inorg. Chem.*, 2014, **53**, 5738-5749.
33. D. L. Rochester, S. Develay, S. Zális and J. A. G. Williams, *Dalton Trans.*, 2009, 1728-1741.
34. R. Babadi Aghakhanpour, S. M. Nabavizadeh, M. Rashidi and M. Kubicki, *Dalton Trans.*, 2015, **44**, 15829-15842.
35. R. Paul, P. Kumbhakar and A. Mitra, *Appl. Surf. Sci.*, 2011, **257**, 6699-6703.
36. L. Hao, M. A. Mansour, R. J. Lachicotte, H. J. Gysling and R. Eisenberg, *Inorg. Chem.*, 2000, **39**, 5520-5529.
37. T. Tuerk, U. Resch, M. A. Fox and A. Vogler, *Inorg. Chem.*, 1992, **31**, 1854-1857.
38. M. Jamshidi, S. M. Nabavizadeh, H. R. Shahsavari and M. Rashidi, *RSC Adv.*, 2015, **5**, 57581-57591.
39. H. Tsubaki, A. Sekine, Y. Ohashi, K. Koike, H. Takeda and O. Ishitani, *J. Am. Chem. Soc.*, 2005, **127**, 15544-15555.
40. A. F. Rausch, L. Murphy, J. A. G. Williams and H. Yersin, *Inorg. Chem.*, 2012, **51**, 312-319.

41. H.-L. Zhang, S. D. Evans, J. Henderson, R. E. Miles and T. Shen, *J. Phys. Chem. B*, 2003, **107**, 6087-6095.
42. B. S. Furniss, A. J. Hannaford, P. W. G. Smith and A. R. Tatchell, *Vogel's Textbook of Practical Organic Chemistry*, Longman Scientific & Technical, 5th edn., 1989.
43. G. M. Sheldrick, *Acta Cryst.*, 2015, **A71**, 3.
44. G. M. Sheldrick, *Acta Cryst.*, 2015, **C27**, 3-8.
45. M. J. Frisch, G. W. Trucks, H. B. Schlegel, G. E. Scuseria, M. A. Robb, J. R. Cheeseman, G. Scalmani, V. Barone, B. Mennucci, G. A. Petersson, H. Nakatsuji, M. Caricato, X. Li, H. P. Hratchian, A. F. Izmaylov, J. Bloino, G. Zheng, J. L. Sonnenberg, M. Hada, M. Ehara, K. Toyota, R. Fukuda, J. Hasegawa, M. Ishida, T. Nakajima, Y. Honda, O. Kitao, H. Nakai, T. Vreven, J. J. A. Montgomery, J. E. Peralta, F. Ogliaro, M. Bearpark, J. J. Heyd, E. Brothers, K. N. Kudin, V. N. Staroverov, T. Keith, R. Kobayashi, J. Normand, K. Raghavachari, A. Rendell, J. C. Burant, S. S. Iyengar, J. Tomasi, M. Cossi, N. Rega, J. M. Millam, M. Klene, J. E. Knox, J. B. Cross, V. Bakken, C. Adamo, J. Jaramillo, R. Gomperts, R. E. Stratmann, O. Yazyev, A. J. Austin, R. Cammi, C. Pomelli, J. W. Ochterski, R. L. Martin, K. Morokuma, V. G. Zakrzewski, G. A. Voth, P. Salvador, J. J. Dannenberg, S. Dapprich, A. D. Daniels, O. Farkas, J. B. Foresman, J. V. Ortiz, J. Cioslowski and D. J. Fox, *Gaussian 09, Revision B.01*, 2010.
46. Chemissian v4.2, 2014, <http://www.chemissian.com>.

Table of Contents Entry

Influence of Thiolate Ligands on Luminescent Properties of Cycloplatinated(II) Complexes

The replacement of chloride ligand in cycloplatinated(II) complexes with various thiolate ligands leads to a profound change in the nature of lowest-energy singlet and triplet excited states.

